

# Efficient Quantum Simulation of Open Quantum System Dynamics on Noisy Quantum Computers

Shin Sun,<sup>1</sup> Li-Chai Shih,<sup>1</sup> and Yuan-Chung Cheng<sup>1, 2, 3, \*</sup>

<sup>1</sup>*Department of Chemistry, National Taiwan University, Taipei City 106, Taiwan*

<sup>2</sup>*Center for Quantum Science and Engineering,*

*National Taiwan University, Taipei City 106, Taiwan*

<sup>3</sup>*Physics Division, National Center for Theoretical Sciences, Taipei City 106, Taiwan*

(Dated: November 13, 2021)

Quantum simulation represents the most promising quantum application to demonstrate quantum advantage on near-term noisy intermediate-scale quantum (NISQ) computers, yet available quantum simulation algorithms are prone to errors and thus difficult to be realized. Herein, we propose a novel scheme to utilize intrinsic gate errors of NISQ devices to enable controllable simulation of open quantum system dynamics without ancillary qubits or explicit bath engineering, thus turning unwanted quantum noises into useful quantum resources. Specifically, we simulate energy transfer process in a photosynthetic dimer system on IBM-Q cloud. By employing designed decoherence-inducing gates, we show that quantum dissipative dynamics can be simulated efficiently across coherent-to-incoherent regimes with results comparable to those of the numerically-exact classical method. Moreover, we demonstrate a calibration routine that enables consistent and predictive simulations of open-quantum system dynamics in the intermediate coupling regime. This work provides a new direction for quantum advantage in the NISQ era.

## INTRODUCTION

Quantum computers promise revolutionary advantages in simulating quantum systems highly important in physics and chemistry.[1] The concept of quantum simulation refers to utilizing quantum computers to simulate other quantum systems of interest with resources much smaller than those required for the same simulation in classical computers, and it could lead to significant breakthroughs for scientific research[2, 3]. Quantum simulation also repre-

sents one of the most critical and successful applications of near-term quantum computers[4]. However, although various quantum simulation algorithms have been proposed[5–7], many of them have limited practical advantages over the classical counterparts due to severe hardware constraints of current quantum devices. Contemporary quantum computers are prototypical noisy intermediate scale quantum (NISQ) devices[8, 9] as they are subjected to various coherent and decoherent noises as well as limited in size and connectivity.

Since fault-tolerant universal quantum computation[10, 11] is unlikely to be available in the near future, we are urged to find problems which are hard to solve on classical computers but suitable for NISQ computers in order to demonstrate quantum advantages for solving real-world problems. The simulation of open quantum systems is one of such problems with significant applications, as dissipative dynamics of open quantum systems[12, 13] play crucial roles in a broad range of physical and chemical phenomena of complex systems, such as photosynthetic light harvesting[14–16], or electron transfer in organic materials[17, 18]. Open quantum systems also stand at the brink of quantum to classical transition, which is of great importance for the fundamentals of quantum theory[19]. Hence, enabling efficient and accurate simulation of open quantum system dynamics could lead to significant advances in both quantum science and technology.

Conventional methods for the simulation of open quantum system dynamics on classical computers, such as the quantum master equation approach[12], are based on certain weak-coupling assumptions about the underlying system-bath interactions. When the assumptions do not hold, non-perturbative treatments such as the numerically exact hierarchical equation of motion (HEOM) method[20–23] become necessary in order to yield accurate results. However, these exact methods on classical computers exhibit extremely steep scaling against the accuracy and system size, which hinders our understanding of the dynamical behaviors of complex open quantum systems.

On the other hand, there exist many proposals to simulating open quantum system efficiently on quantum computers based on explicit engineering of the system-bath interactions.[24–33] For example, Maniscalco *et al.*[24] proposed to simulate the quantum Brownian motion by engineering an artificial reservoir coupled to a single trapped ion, and Barreiro *et al.*[25] suggested to simulate dissipative systems on trapped-ion architectures though the usage of ancillary qubits and optical pumping techniques. In addition, Aspuru-Guzik and coworkers[26] proposed an superconducting analog open quantum simulator for

Fenna-Matthews-Olson complex, where the required system-bath interactions are introduced through explicit engineering of qubit-resonator couplings. Recently, Wang *et al.* [28] proposed a NMR-based quantum simulation of exciton systems with the dephasing noises generated by stochastically-modulated control field. However, due to the necessity of either precise multi-qubit control or explicit system-bath engineering, the resources overhead for these simulation algorithms are still formidable for current quantum devices.

Let us recall Feynman in his famous quote [34]:

"Nature isn't classical, dammit, and if you want to make a simulation of nature, you'd better make it quantum mechanical, and by golly it's a wonderful problem, because it doesn't look so easy."

In the same spirit, we might as well simulate dissipative quantum dynamics using intrinsic noises in quantum computers. In this work, we propose to simulate open quantum system dynamics on quantum computers by directly exploiting the errors generated on the gate level in superconducting NISQ devices, which is an idea that strongly differs from existing proposals. The idea of utilizing decoherence and thermal effects in quantum computers to simulate quantum dynamics was previously suggested by Lloyd and coworkers[35], but the idea has never been realized. For most quantum algorithms, quantum noises are undesirable and destructive. Nevertheless, we recognize that the decoherence effects induced by quantum noises are necessary and can be used as resources for simulations of open quantum systems. Our approach thus does not require explicit engineering of the control field, and no extra qubits for modeling the environment are needed either.

In this paper, we demonstrate that gate errors on IBM-Q cloud quantum computers can be controlled and utilized to simulate excitation energy transfer (EET) dynamics in a molecular exciton dimer system under tunable dissipative environments, and we compare the simulation results with HEOM calculations to validate that they correspond to dynamics induced by realistic system-bath interactions. We also show that quantum computer can quantitatively predict quantum dissipative dynamics at the intermediate system-bath coupling regime that are hard to simulate accurately with classical methods. Moreover, since the device instability for both qubit and quantum gates is still high for NISQ computers[36, 37], we demonstrate designed calibration routines for noise strengths to achieve consistent simulations. In summary, our approach shows the possibility of utilizing NISQ devices as quantum

noise generators as well as embracing the noises to simulate physical systems. This opens new directions for the simulation of open quantum system dynamics and various stochastic systems such as in biology, finance, or cryptography.

## RESULTS

### Exciton Model for Excitation Energy Transfer

To demonstrate the simulation of open quantum system dynamics on noisy quantum computers, we adopt a simple exciton model that describes EET in photosynthetic systems. In the model, physical systems are represented as different monomers called "sites", which constitute the whole complex, and two quantum states, the ground state and the excited state, are considered for each site. This two-level property makes them mapped naturally to qubits, and thus ideal target systems to be simulated on quantum computers. The Hamiltonian describing an excitonic system with  $N$  sites in the second-quantized form is

$$H = \sum_{i=1}^N \epsilon_i a_i^\dagger a_i + \sum_{i \neq j=1}^N J_{ij} a_i^\dagger a_j \quad (1)$$

where  $a_i^\dagger(a_i)$  is the creation (annihilation) operator acting on site  $i$ . It is convenient to introduce the state  $|0\rangle$ , which corresponds to the state with all sites in the ground state, and  $|i\rangle = a_i^\dagger|0\rangle$ , which corresponds to the state with a single excitation at site  $i$  while other sites are in the ground state. The diagonal matrix element  $\epsilon_i$  is the site-energy of  $|i\rangle$ , and the off-diagonal term  $J_{ij}$  corresponds to excitonic coupling between  $|i\rangle$  and  $|j\rangle$ . For simplicity, we consider a symmetric dimer system ( $N = 2$ ,  $\epsilon_1 = \epsilon_2 = 0$ ) with excitonic coupling  $J_{12} = J_0$ . This model also corresponds to the spin-boson problem or the Heisenberg XY model for magnetism[38]. In this work, we specifically focus on the dynamics in the one-exciton manifold for EET.

To represent and propagate the exciton dynamics efficiently on quantum computers, we encode the exciton occupancies of the dimer system in the computational basis of two qubits. The Hamiltonian of the system is mapped to Pauli operators acting on the qubit Hilbert space via a Jordan-Wigner type transformation (see Methods); thus, the quantum circuit which simulates the system propagator  $e^{-iHt}$  ( $\hbar = 1$ ) can be constructed as shown in

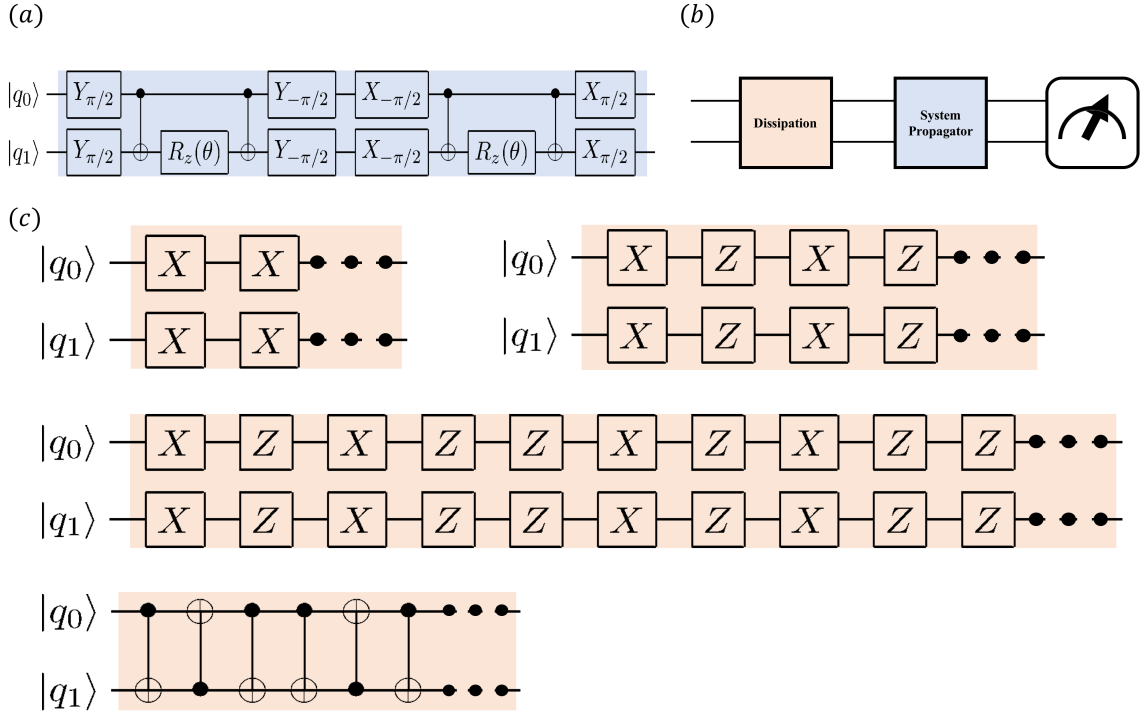


FIG. 1. **Quantum circuits for the dissipative quantum system simulation.** (a) The circuit implementing the time-evolution propagator for the unbiased exciton dimer in our experiments. (b) Illustration of the simulation scheme. The full simulation circuit first undergoes dissipative operation via different decoherence-inducing gates that introduce decoherence into the simulated system, and followed by the propagator of the system Hamiltonian. (c) Various decoherence-inducing gate sequences used for the dissipation circuit.

Fig. 1 (a), where  $\theta$  corresponds to the simulation time. Note that the resulting circuit for the propagator is exact in the symmetric dimer case due to the commutativity of the two terms in the system Hamiltonian. In a general biased excitonic system, one has to build the propagator through Trotterization or other more efficient state propagation schemes[39]. To retrieve the dynamical population information, we perform projective measurements in the qubit computational basis, and renormalize the probabilities within the one-exciton manifold (see Methods) to compensate for the leakage errors.

We experimentally simulated the time evolution of the dimer system with initial population on site 1 using the quantum circuit depicted in Fig. 1(a) on the IBM-Q superconducting quantum computers[40]. Figure 2 depicts the simulated population dynamics. The results show a perfect coherent Rabi oscillation ("quantum beating"). This validates the mapping

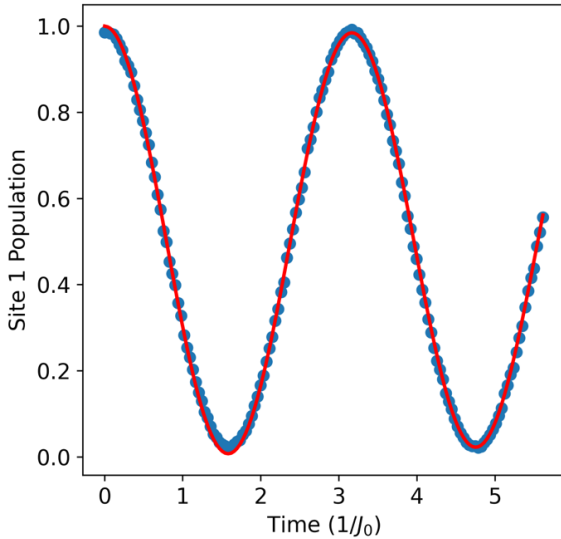


FIG. 2. **Simulated coherent dynamics of the dimer system.** Population on site 1 as a function of time is depicted when the system is initially prepared as  $|\psi(0)\rangle = |1\rangle$ . The simulation result obtained on `ibmq_bogota` (blue dots) and a cosine function (red line) are both shown.

and confirms that our renormalization procedure to account for the leakage error does not affect the coherence in the one-exciton manifold.

#### Decoherence Engineering by Prepending Identity Gate Sequences

To simulate realistic energy transfer dynamics on IBM-Q systems, we aim to utilize intrinsic imperfections in the quantum gates to model a dissipative environment in a controllable manner. To this end, we prepend a dissipation part to the simulation circuit by a number of gate sequences that ideally contract to the identity gate (Fig 1(b)). Due to the gate errors, the identity gate sequences will introduce quantum noise into the simulation on NISQ devices. We thus refer to them as "decoherence-inducing" gates in this work. The system propagator then changes the frame of the system from the interaction picture to Schrödinger picture at a given simulation time. Finally, projective measurements are performed to monitor site populations.

To tune the strength of system-bath couplings, we control the number of decoherence-inducing gates applied per unit simulation time. Therefore, we define a damping coefficient

$d = \frac{N_I}{t/\Delta T_D}$ , where  $t$  is the total simulation time,  $\Delta T_D$  is the decoherence period, and  $N_I$  is the number of decoherence-inducing gates applied. The damping coefficient can then be adjusted in the quantum simulation to realize different system-bath coupling strengths.

Regarding decoherence-inducing gates, we examined four types of identity gate sequences as shown in Fig. 1(c), including 1.  $(X)^2$  2.  $(XZ)^2$  3.  $(XZXZZ)^2$  4.  $(SWAP)^2$ . Gate sequences 1-3 act on a single qubit, while gate 4 is a non-local gate. These gate sequences are chosen based on a series of preliminary studies on noisy qubit dynamics induced by various quantum gates available on the IBM-Q systems (see Sec. S1-S5 in the SI). We noted that because the virtual-Z gate implementation on IBMQ systems [41] corresponds to a mere frame shift of the subsequent pulses, it does not introduce a real time elapse in the simulation (i.e. no pulse is applied). Hence, Z gates cannot introduce gate noises (Fig. S6). We therefore choose X gate as our primary decoherence-inducing single-qubit gate. In the following, we systematically analyze the dissipative dynamics induced by the four types of gate sequences, and details of the implementation and parameters used in this work are given in the Methods section.

### Dissipative Dynamics Induced by Single-qubit Gate Sequences

Three types of single-qubit gate sequences are examined in this work. We first employ  $(X)^2$  gates to simulate EET dynamics of the model dimer system. Figure 3 shows the simulated population dynamics at four different damping coefficients. At small damping coefficients ( $d = 20$  and  $d = 30$ ), the decoherence of the quantum beating is apparent and becomes more pronounced as  $d$  increases, which are in line with our proposal. However, at larger damping coefficients ( $d = 50$  and  $d = 70$ ), the population dynamics exhibit unphysical multifrequency behavior and large population revival; thus, the simulated dynamics cannot reach equilibrium and do not correspond to physical dissipative dynamics. These results indicate that  $(X)^2$  does not introduce realistic decoherence effects into the EET dynamics and thus cannot be used as a proper decoherence-inducing gate.

To elucidate the errors accompanying the  $(X)^2$  gate sequence, we performed state tomography after applying  $(X)^2$  gates on a single qubit initialized at a given each basis state to analyze the dynamics induced (see Sec. S1-S4 in the SI). Figure S3 indicates that  $(X)^2$  error consists of significant over-rotation of the X gate, which leads to a systematic drift in the

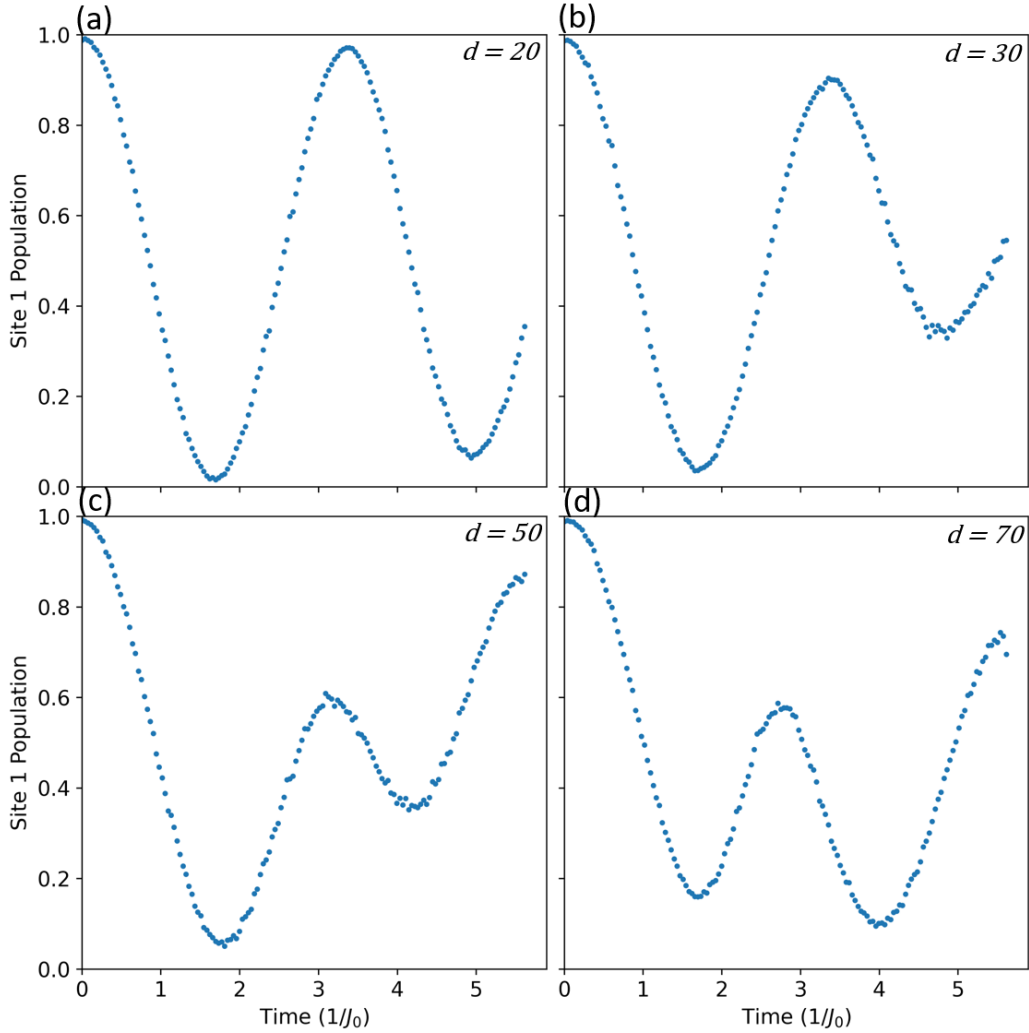


FIG. 3. **Simulated dissipative dynamics induced by  $(X)^2$ .** We plot the population on site 1 (blue dots) as a function of time at 4 different damping coefficients. The decoherence effects are induced by applying the  $(X)^2$  gates. (a)  $d = 20$ , (b)  $d = 30$ , (c)  $d = 50$ , and (d)  $d = 70$ . Experiments were performed on `ibmq_bogota`.

dynamics and thus produces non-physical results in the EET simulation. In other words, applying  $(X)^2$  gates results in the simulation of an effective Hamiltonian that is different from the target Hamiltonian. The issue could have been resolved by adding an offset to each X rotation to counteract the over-rotation, but the downside is that the over-rotation angle is then needed for each experiment beforehand, which is not practical given that the stabilities of the available quantum computers are still less than perfect.

In order to eliminate the drift in the X gate error and obtain more consistent random

noises, we employ echo-type equivalents to the  $(X)^2$  gate, the  $(XZ)^2$  gate, and the corresponding higher order  $(XZXZZ)^2$  gate as the decoherence-inducing gates. The design of these gates is related to the compensating pulse sequence techniques[42] (see Sec. S5 in the SI), which dynamically correct the X over-rotation. Figures S7 and S8 show the time-evolution of a single qubit induced by the  $(XZ)^2$  and  $(XZXZZ)^2$  gates, respectively. Due to the phase error, the  $(XZ)^2$  does not remove the over-rotation completely. Nevertheless, the  $(XZXZZ)^2$  sequence clearly induces a depolarization-like random noise, and it can thus be used to model a physical decoherence process.

In the results shown in Fig. 4, we employed  $(XZXZZ)^2$  as the decoherence-inducing gate, and assess the population dynamics for the EET process under different damping coefficients. The decoherence effect can be seen in the damping of the quantum beating, and the decay rate increases with the increase of damping coefficient consistently. This confirms that the  $(XZXZZ)^2$  can be used as a decoherence-inducing gate sequence to introduce quantum noises into the simulation. However, even when the damping coefficient is large ( $d = 35$ , where the circuit depth is closed to the device limit), the population dynamics still remain coherent, and this restricts us from exploring the EET dynamics in the incoherent regime. Furthermore, the maximum time duration of the simulation is limited by the deepest circuit depth available on the NISQ devices. As  $d$  increases, the number of gates needed to perform simulation in a unit time also increases, which limits the available simulation time. Therefore, a more general decoherence-inducing gate sequence is desirable.

### Dissipative Dynamics under $(SWAP)^2$ Gate Sequences

In addition to single-qubit gates, two-qubit gates could also be utilized to construct decoherence-inducing gate sequences. We discovered that the non-local  $(SWAP)^2$  gates on IBM-Q systems can introduce consistent decoherence effects into the model system and drive the system towards equilibrium efficiently. In Fig. 5, the population dynamics under  $(SWAP)^2$  with different damping coefficients for the model system are depicted. The decay of the quantum beating is much faster compared to results shown in Fig. 4, suggesting that the noise introduced by the  $(SWAP)^2$  gate is stronger than that introduced by the  $(XZXZZ)^2$  gate. The system even exhibits incoherent transfer dynamics at a large  $d$  (Fig. 5(d)), which enable us to study the dissipative dynamics in the strong coupling regime.

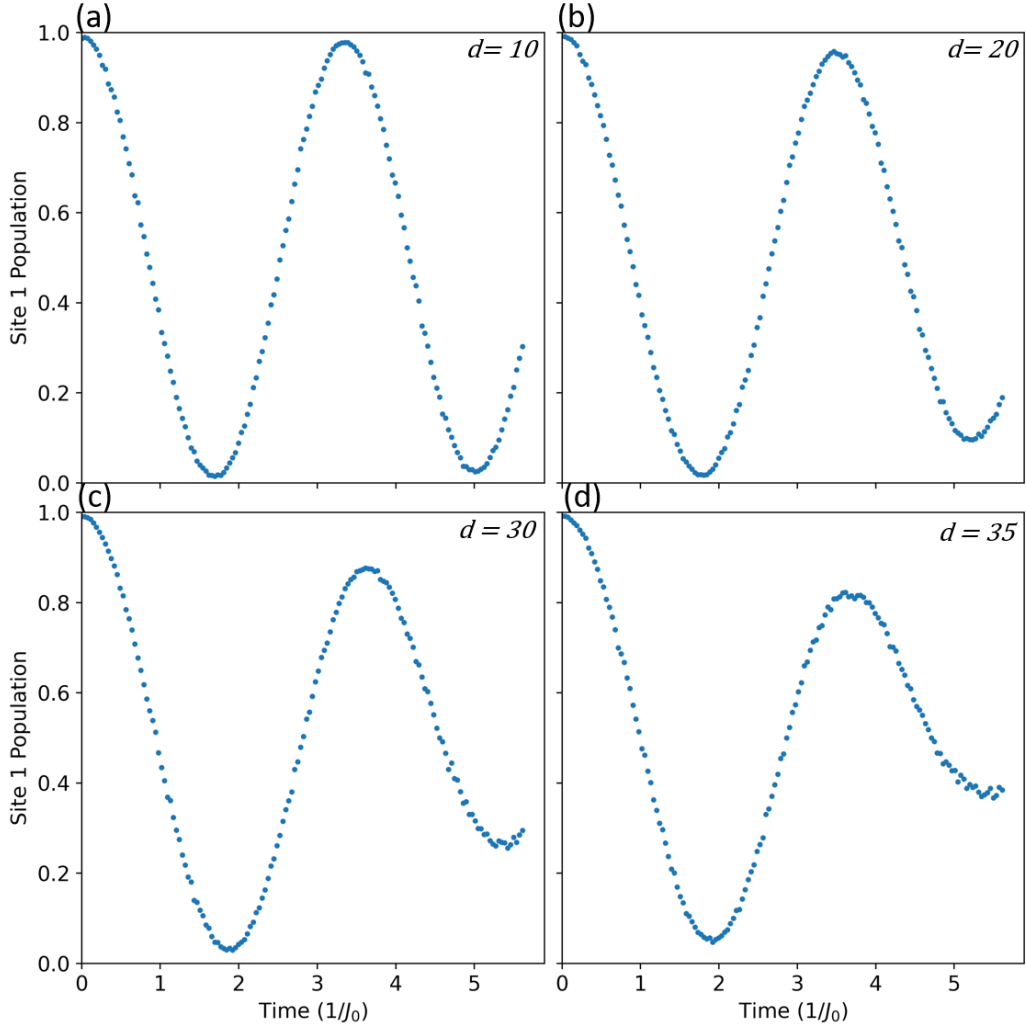


FIG. 4. **Simulated dissipative dynamics induced by  $(XZXZZ)^2$ .** We plot the population dynamics on site 1 as a function of time under 4 different damping coefficients. The decoherence effects are induced by applying the  $(XZXZZ)^2$  gates. (a)  $d = 10$ , (b)  $d = 20$ , (c)  $d = 30$ , and (d)  $d = 35$ . Experiments were performed on `ibmq_bogota`.

Since the dissipative dynamics under  $(SWAP)^2$  gates are consistent throughout coherent to incoherent regime, we quantitatively analyze and compare them to realistic open quantum system dynamics. The possibility of combining different type of gate sequences or other pulse-level techniques to achieve finer control over system-bath couplings is left for future research.

We first extract the population transfer rate by fitting the dynamics at each damping coefficient with an exponential-cosine function, and plot the rates against the damping

coefficients (Fig. 6). The relation between decay rate and damping coefficient varies under different system-bath coupling strengths. At weak system-bath couplings (small damping coefficients), the decay rate approximately increases linearly with respect to the damping coefficient ( $d = 0$  to  $d = 10$ ); however, as the damping coefficient further increases ( $d > 10$ ), the rate exhibits a turnover behavior. It is interesting and important to note that the relation is not monotonic, suggesting an optimal transfer rate at the intermediate coupling regime in accordance with previous EET studies[22, 43, 44]. The behavior also suggests that our simulation results are non-trivial in the sense that they cannot be reproduced by simple Redfield-type theories. Note that the computational costs in terms of number of qubits and circuit depth needed in our proposed scheme are linear with respect to the number of sites ( $N$ ) and simulation time ( $t$ ), respectively. Moreover, the dissipative part can be introduced by using at most two-qubit gates that can be executed in parallel on nowadays superconducting quantum computers. Thus, the proposed scheme should be able to be easily scaled up to simulate open quantum system dynamics for multiple-site systems.

### Comparison with Numerically Exact HEOM Simulations

To validate that our simulation based on  $(SWAP)^2$  decoherence-inducing gate represents dynamics of a realistic open quantum system, we compare our results to those obtained by classical computation based on a microscopic modeling of system-bath interactions. To this end, we fit our quantum simulation data to those obtained from the hierarchical equation of motion using the Parallel Hierarchy Equations of Motion Integrator program[45] on classical computers. The HEOM method employs a Drude-Lorentz type spectral density to model system-bath interactions:

$$J(\omega) = \frac{\lambda}{2} \frac{\gamma\omega}{\gamma^2 + \omega^2} \quad (2)$$

where  $\lambda$  is the reorganization energy, representing the system-bath coupling strength, and  $\gamma$  is the cut-off frequency that corresponds to the inverse bath relaxation time scale. HEOM has been recognized as a highly accurate method for EET dynamics; however, the full HEOM method requires solving a system of non-polynomial number of differential equations. As a result, HEOM calculations need truncation at a certain hierarchical level and exhibit extremely stiff computational cost against system size, making it best suited for small-size

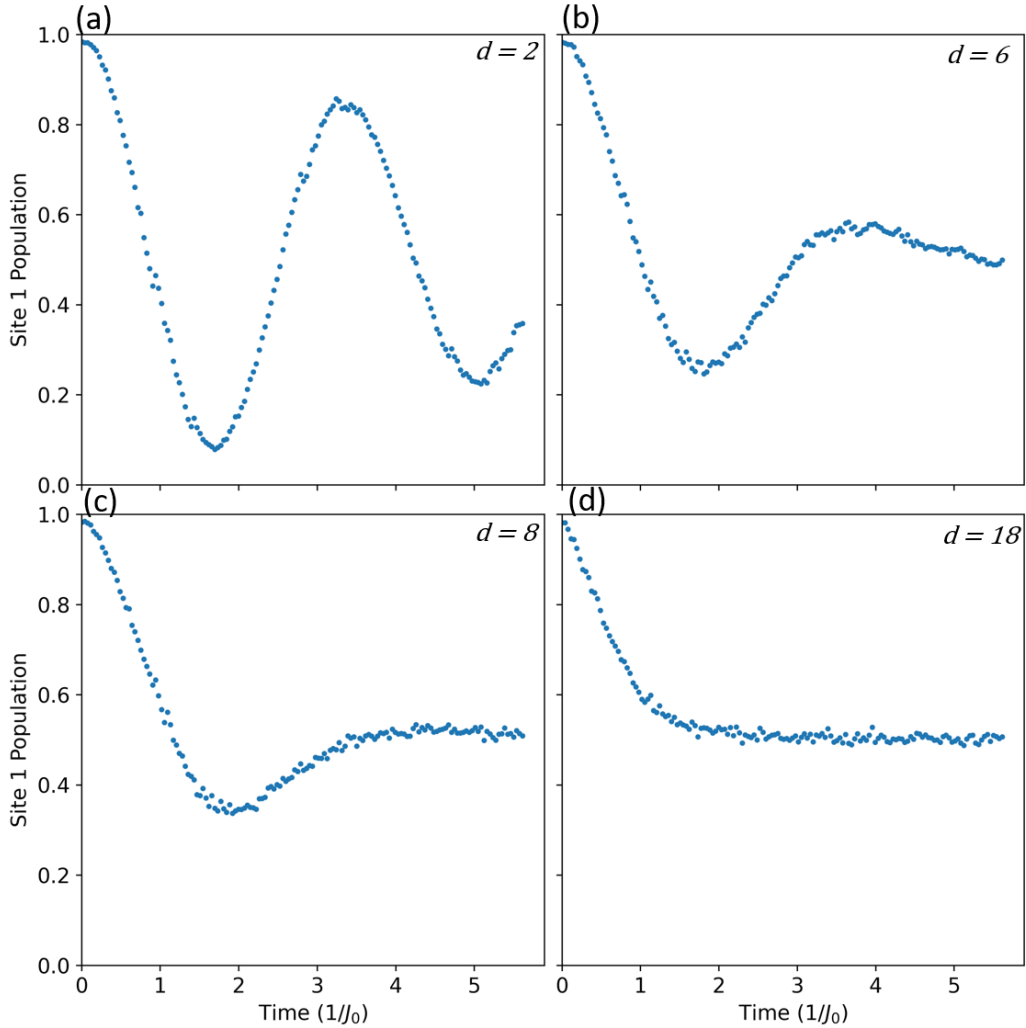
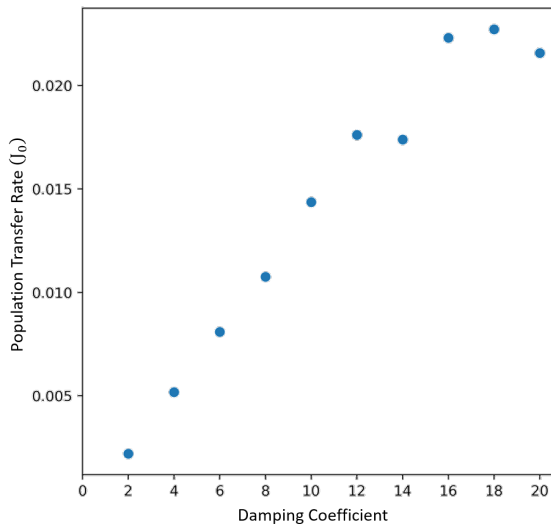


FIG. 5. **Simulated dissipative dynamics induced by  $(SWAP)^2$ .** We plot the population dynamics on site 1 as a function of time under 4 different damping coefficients. The decoherence effects are induced by applying the two-qubit  $(SWAP)^2$  gates. (a)  $d = 2$ , (b)  $d = 6$ , (c)  $d = 8$ , and (d)  $d = 18$ . Experiments were performed on `ibmq_paris`.

systems.

We choose to fit HEOM dynamics to the dynamics simulated using the  $(SWAP)^2$  decoherence-inducing gates at two cases, a weak coupling case with  $d = 2$  and a strong coupling case with  $d = 18$ . For the HEOM model parameters adopted in the fitting, we assume that each site in the dimer is coupled to identical and independent baths, and fix  $J_0 = 100 \text{ cm}^{-1}$ ,  $\gamma = 100 \text{ ps}^{-1}$ , and the temperature at 300 K. We only vary  $\lambda$  in the HEOM model to reproduce the simulated dynamics using  $(SWAP)^2$  gates on IBM-Q systems.



**FIG. 6. Simulated population transfer rate as a function of damping coefficient.** Blue dots depict population transfer rate from  $|1\rangle$  to  $|2\rangle$  extracted from quantum simulation using  $(SWAP)^2$  as decoherence-inducing gate sequence at different damping coefficients. Experiments were performed on `ibmq-paris`

In Fig. 7(a) and Fig. 7(b), we compare the population dynamics simulated on the IBMQ devices with the best HEOM fit for the  $d = 2$  and  $d = 18$  cases, respectively. The optimal HEOM parameters are listed in Table. I. The results demonstrate that both coherent and incoherent EET dynamics simulated by the  $(SWAP)^2$  decoherence-inducing gates on IBMQ devices can be quantitatively reproduced by microscopic HEOM calculations. Evidently, our proposed scheme can simulate realistic dissipative quantum dynamics with controllable system-bath coupling strengths.

Furthermore, the excellent agreement between dissipative dynamics induced by  $(SWAP)^2$  gates and HEOM simulation of a microscopic model system provides crucial insights into the characteristics of the errors induced by the  $(SWAP)^2$  gates. The Drude-Lorentz bath model adopted in the HEOM method represents an overdamped Brownian bath with Gaussian random fluctuations, and it should not be too surprising that the gate errors in IBM-Q systems could be quantitatively described by such a random process. In this regard, the fit to HEOM dynamics provides a consistent framework to extract error characteristics in quantum gates implemented in a quantum computer, as shown in the bath parameters listed

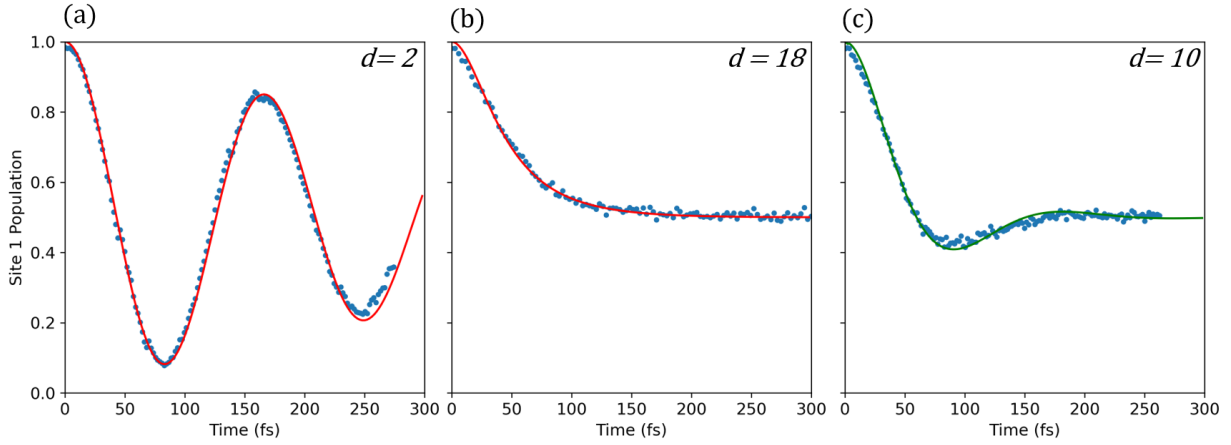


FIG. 7. **HEOM analysis of the simulated dynamics induced by  $(SWAP)^2$  gates.** The simulated population dynamics at three system-bath coupling parameters are shown: (a) weak coupling ( $d = 2$ ), (b) strong coupling ( $d = 18$ ), and (c) intermediate coupling ( $d = 10$ ). The weak- and strong-coupling results are fitted individually with HEOM simulations, of which the results are shown as red lines and the fitting parameters are listed in Table I. With the fitted data, we assume a linear relationship between the reorganization energy and damping coefficient, and use quantum simulation to predict the dynamics at  $\lambda = 120 \text{ cm}^{-1}$ . The predicted dynamics and the corresponding HEOM dynamics are shown as dots and the green line, respectively, in (c).

in Table I. Such characteristics could be dependent on the type of decoherence-introducing gates as well as the hardware, and could have significant implications in optimizations of quantum algorithms and even designs of quantum error-correction schemes. This direction of research is a work in progress and will be reported in another paper.

Knowing that the simulation scheme has worked, we then investigate if we could use the scheme to predict the dissipative dynamics at other system-bath coupling strengths by controlling the damping coefficient. To this end, we assume a linear relationship between damping coefficient and bath reorganization energy in the microscopic model. According to Table I, we can determine the required damping coefficient used in the quantum simulation for simulating dynamics with a given reorganization energy. For instance, a model system with  $\lambda = 120 \text{ cm}^{-1}$  should correspond to the quantum simulation with  $d = 10$ . In Fig. 7(c), we plot the simulated dynamics at  $d = 10$  and the HEOM result with  $\lambda = 120 \text{ cm}^{-1}$ . Note that there are no free parameters in both simulation shown here. The excellent agreement

TABLE I. The fitted HEOM parameters for the dissipative dynamics shown in Fig. 7.

	Underdamped	Overdamped
Damping coefficient	2	18
Excitonic coupling	$100 \text{ cm}^{-1}$	$100 \text{ cm}^{-1}$
Cutoff frequency	$100 \text{ ps}^{-1}$	$100 \text{ ps}^{-1}$
Reorganization energy	$15 \text{ cm}^{-1}$	$227 \text{ cm}^{-1}$
Hierarchy truncation	8	8
Temperature	300 K	300 K

between them provides strong numerical evidence to support that the proposed scheme for dissipative quantum dynamics simulation can be used as a predictive tool, especially in the difficult intermediate coupling regime.

### Temporal Stability and Calibration Scheme

During our study, we also found that the gate noises on IBM-Q superconducting devices in general could vary on a daily basis (see Sec. S6 in the SI). Therefore, it is crucial that we assess the stability of our scheme on different days. We thus performed on different days a series of simulations of the EET dynamics using  $(SWAP)^2$  gates with different damping coefficients, and for each damping coefficient we fit the simulated population dynamics with HEOM calculations to analyze the relationship between the fitted reorganization energies and damping coefficients. In Fig. 8, we plot the calibration curves of the fitted reorganization energies against the damping coefficients for two separated sets of simulations executed on different days. We observe that the two curves remain linear, yet their slopes are different, which indicates that the device shows different level of noise strength in different days, and it could affect our simulation significantly.

Nevertheless, the linear relationship for the calibration curve on each day suggests that it is possible to run a small number of experiments to calibrate the noise strengths. Ideally, two experiments, one for a weak coupling case and the other for a strong coupling case, could be carried out and fitted to classical simulations to determine the noise characteristics. Note that accurate methods to simulate the dynamics in these two extremes are not as costly

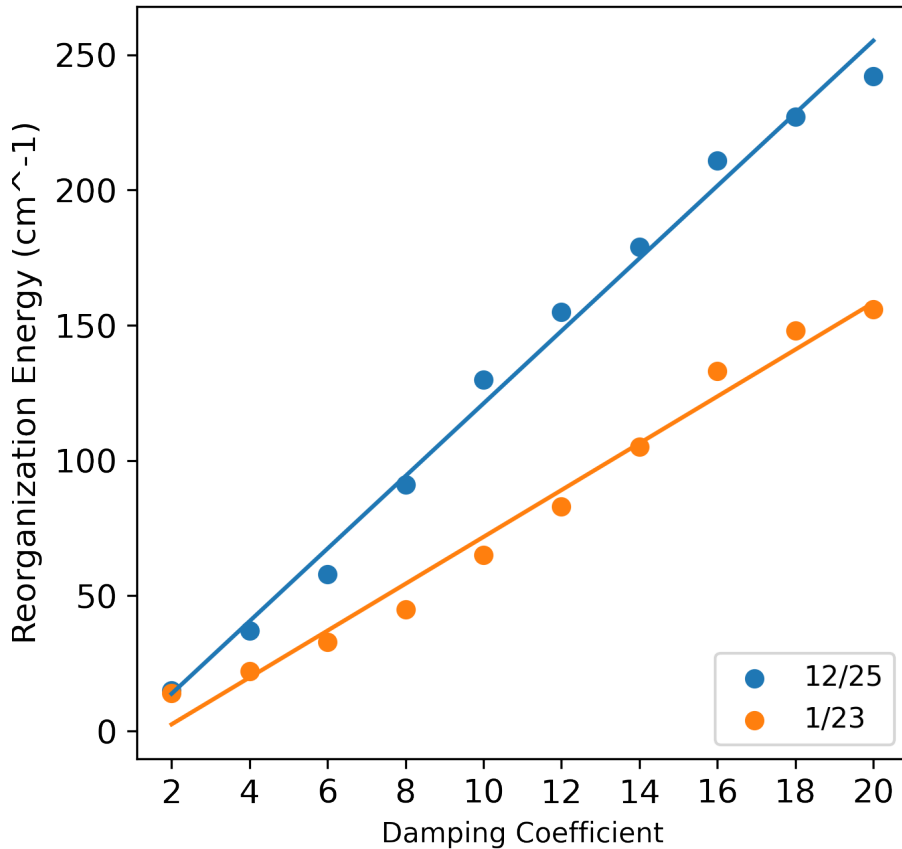


FIG. 8. **Calibration curves on different days.** We plot the reorganization energy obtained from HEOM fitting against the damping coefficient used to generate quantum simulation data for experiments performed on different days. Blue dots denote results obtained on 2020/12/25, and yellow dots are results obtained on 2021/1/23. All experiments were performed on `ibmq-paris`.

as simulating dynamics at the intermediate coupling regime [12], and therefore the HEOM method is not strictly required if a large system is under study. The relation can then be used to simulate dissipative dynamics under other system-bath coupling strengths by controlling only the damping coefficient on quantum computers. The fluctuation of noise strengths for the single-qubit decoherence-inducing gates is discussed in Sec. S6 in the SI. Other methods to efficiently calibrate the noise strengths and, possibly, stabilize them are left for further research.

## DISCUSSION

In this work, we have successfully simulated the EET dynamics for a symmetric dimer system under different damping regimes using only the intrinsic gate noises of the IBM-Q systems. Our approach requires neither additional ancillary qubits to represent the environment nor explicit bath engineering on the hardware level. Significantly, we show that by designing gate sequences to produce consistent random noises, the simulation scheme can yield results that are in excellent agreement with HEOM simulations of microscopic EET models. Moreover, although current superconducting quantum devices does not offer enough stability over time for consistent quantitative simulation of dissipative quantum dynamics, we show that a simple calibration scheme can be applied to turn NISQ devices into a controllable simulator for open quantum system dynamics to successfully predict the EET dynamics in the intermediate coupling regime.

In principle, the decoherence-inducing gate method proposed here only needs  $N$  qubits to simulate dissipative dynamics of a  $N$ -site system, and with superconducting quantum computer with more than 100 qubits readily available in the near future, it is possible to use our method to simulate large and complex excitonic system such as the photosynthetic photosystem I ( $\sim 100$  sites) and photosystem II supercomplex ( $\sim 300$  sites), as well as conjugated polymers and a matrix of small-molecule chromophores used in organic solar cells. Realization of such simulations could significantly advance our understanding of elementary photophysical processes on these crucial systems. On the other hand, accurate classical simulation methods such as the HEOM approach demand significantly more computational cost and can not be easily applied to systems  $>100$  sites. Generally speaking, with extremely efficient coding and parallel algorithmic optimization, the HEOM method could be applied to simulate a system with about 50 sites, but further scaling up would be formidable. Therefore, we present a quantum simulation algorithm that is highly likely to demonstrate clear quantum advantage in the near future. Note that the advantages comes naturally from using NISQ devices as a quantum noise generator, and our study indicates that the task is not trivial as nowadays NISQ devices could exhibit coherent noises that are not described by simple stochastic processes. The key insight in this work is that by choosing and designing specific compensating pulse sequences, purely random gate errors can be realized and controlled. Hence, intrinsic gate errors could and must be engineered to become a type

of quantum resources.

We believe that the major roadblock of the scheme proposed in this work remains the limited circuit depth available on nowadays NISQ devices. We noted that there exists a slight discrepancy between simulated dynamics and HEOM fitting at long time for the dynamics shown in Fig. 7(a), which can be attributed to accumulated errors in the deep quantum circuit needed to simulate long time dynamics. One possible method to remedy this inaccuracy in the long time dynamics is to use the transfer tensor algorithm[46] to tease out dynamical correlations in quantum simulation at the initial stage, and propagate the dynamic classically to an arbitrary long time. Such hybrid quantum-classical approach would only need shallow quantum simulations and could make it possible to overcome the circuit depth problem. Of course, traditional transfer tensor algorithm needs dynamical map at each time step, and building up dynamical maps requires process tomography[47] on quantum computers. That makes the scaling not ideal for large system. Thus, we envision that a more compact scheme to obtain dynamical maps based on partial information of the underlying dynamics like compressed sensing techniques[48, 49] should be used if one is to extend the initial trajectories of the dissipative simulation of dynamics based on our scheme.

Our research also suggests a number of possible improvements. First of all, we only explored a controllable bath parameters that is the reorganization energies  $\lambda$ . It is important that a systematic procedure to adjust the cutoff frequencies  $\gamma$  can be found in order to generate baths with any desirable spectral properties. Presumably, dynamics with different  $\gamma$  can be simulated by designing different decoherence-inducing gates or by choosing a different unit-less energy scaling. Furthermore, additional research directions including detailed characterization of the effects of various decoherence-inducing gates, finer control over bath parameters using different gates or pulse level control (like pulse stretching), scheme to provide classically hard-to simulate quantum noises, implementing finite temperature effect for biased exciton systems, and extending the simulations scheme to study larger systems with multiple sites could be foreseen to answer open questions with significant implications.

Interestingly, following the investigation of various decoherence-inducing gates, we also extract important characters of the gate noises. For example, we reveal that a large portion of  $(X)^2$  gate errors consists of over-rotation (see Sec. S4 in the SI). This "off-set" type of error might not as harmful as decoherent errors to quantum computers, because it could have been eliminated by more precise calibration of the pulses or adopting compensating pulse

sequences like our design. However, conventional benchmark protocols only yields highly averaged metrics such as the average gate fidelity for the calibration of gate performance, which would provide limited information to properly describe the composition of the gate noises. Thus, we emphasize that the detailed characterization of the noises in current NISQ devices such as the analyses presented in the SI is still of vital importance for the design of error-mitigation or calibration protocols for quantum simulations.

Finally, we emphasize that the proposed decoherence-inducing gate sequences could serve as well-behaved quantum noise generator that may also be useful for other applications such as state preparation or dissipative quantum computation. We conclude that our results show the possibility of turning NISQ devices into extremely useful and programmable platforms to study open quantum systems under complicated system-bath interactions, and hopefully, can help us investigate complex dynamics in open quantum systems beyond what classical computers can do for us.

## METHODS

### Encoding and Propagating the Exciton Hamiltonian

To encode the Hamiltonian of the exciton dimer system in a quantum computer, a Jordan-Wigner type transformation[50] is used. There, the preparation step is trivial as the state preparation circuit for exciton state with site 1 or 2 being excited can be easily implemented as shown in Fig. 9. Regarding mapping of the Hamiltonian, the second-quantized operators in (Eq. 1) is mapped to the Pauli operators acting locally on qubits according to (Eq. 3)

$$\begin{aligned} a_n^\dagger a_n &= \frac{1}{2}(I_n - Z_n), \\ a_n^\dagger a_m + a_m^\dagger a_n &= \frac{1}{2}(X_m X_n + Y_m Y_n), \quad \forall m \neq n \end{aligned} \quad (3)$$

In our simulation, we model a symmetric dimer with  $J_{12} = J_0$ , therefore we can encode the unit-less  $J = 1$  case without loss of generality. In this case, the simulation time has a derived unit of  $1/J_0$ . The qubit Hamiltonian can then be represented as

$$H = \frac{1}{2}(X_1 X_2 + Y_1 Y_2) \quad (4)$$

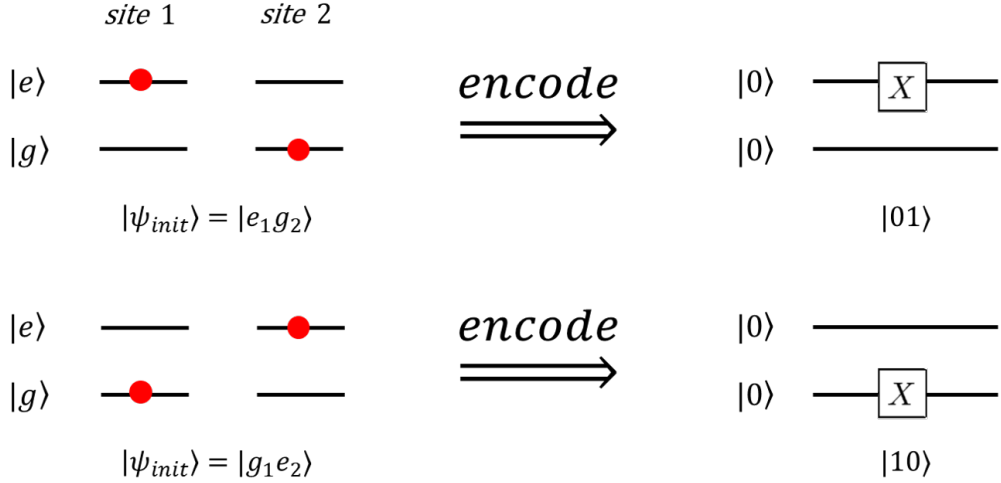


FIG. 9. **Encoding the exciton states in site basis on quantum computers** The preparation of initial state as  $|1\rangle$  or  $|2\rangle$  is implemented by applying an X gate to the corresponding qubit.

To implement the time evolution operator  $e^{-iHt}$  on quantum computers ( $\hbar = 1$ ), one can concatenate propagators for the local term. (Fig. 1(a)). The rotation angle  $\theta$  of the phase gate  $R_z(\theta)$  corresponds to the simulation time. In all our simulation of population dynamics, we set a single time step to be  $\delta\theta = 0.03767$ . (This corresponds to a step of 2 fs for a symmetric dimer system with excitonic coupling =  $100\text{cm}^{-1}$ ). The decoherence period ( $\Delta T_D$ ) is chosen to be  $25\delta\theta$ , i.e. when  $d=1$ , an identity gate sequence is prepended in the dissipation part for each 25 time steps.

### IBM Quantum Experience

All the experiments are performed on superconducting quantum computers provided by IBM quantum experience[40] via qiskit framework[51]. Each job for the simulation of population dynamics consists of 150 circuits corresponding to evenly spaced simulation time. The logical-to-physical qubit mapping layout is chosen so that the CNOT interaction can be directly implemented. The qubit bit string is in little-endian format in accordance with the qiskit convention.

### Population Dynamics from Projective Measurements

To obtain the population in the site basis, we perform projective measurements up to 8192 times in qubit computational basis at each simulation time step, and calculate the population according to  $P_1(t) = \frac{N_{01}(t)}{N_{01}(t) + N_{10}(t)}$ . where  $N_{01}$ , and  $N_{10}$  are counts for the states collapsed to  $|01\rangle$ ,  $|10\rangle$ , respectively. The counts for states collapsed to  $|00\rangle$ ,  $|11\rangle$  are excluded because they are generated by the leakage of population to space outside of the one-exciton manifold.

### ACKNOWLEDGMENTS

We thank IBM and IBM-Q Hub at NTU for accessing quantum devices through IBM Quantum Experience. YCC thanks the Ministry of Science and Technology, Taiwan (Grant No. MOST 109-2113-M-002-004 and MOST 109-2113-M-001-040), Physics Division, National Center for Theoretical Sciences (Grant No. 110-2124-M-002-012), and National Taiwan University (Grant No. 109L892005) for financial support.

### COMPETING INTERESTS

The authors declare no conflict of interest.

### AUTHOR CONTRIBUTIONS

S. Sun and Y.-C. Cheng conceived the project. S. Sun and L.-C. Shih designed and performed the experiments. S. Sun, L.-C. Shih, and Y.-C. Cheng contributed to the manuscript.

---

\* Email: yuanchung@ntu.edu.tw

- [1] Michael A Nielsen and Isaac Chuang. *Quantum computation and quantum information*. Cambridge University Press, 2010.
- [2] Dave Bacon, Andrew M Childs, Isaac L Chuang, Julia Kempe, Debbie W Leung, and Xinlan Zhou. Universal simulation of markovian quantum dynamics. *Phys. Rev. A*, 64:062302, 2001.
- [3] Iulia M Georgescu, Sahel Ashhab, and Franco Nori. Quantum simulation. *Rev. Mod. Phys.*, 86:153, 2014.
- [4] Ehud Altman, Kenneth R Brown, Giuseppe Carleo, Lincoln D Carr, Eugene Demler, Cheng Chin, Brian DeMarco, Sophia E Economou, Mark A Eriksson, Kai-Mei C Fu, et al. Quantum simulators: Architectures and opportunities. *PRX Quantum*, 2:017003, 2021.
- [5] Man-Hong Yung, James D Whitfield, Sergio Boixo, David G Tempel, and Alan Aspuru-Guzik. Introduction to quantum algorithms for physics and chemistry. *Adv. Chem. Phys.*, 154:67–106, 2014.
- [6] Sam McArdle, Suguru Endo, Alan Aspuru-Guzik, Simon C Benjamin, and Xiao Yuan. Quantum computational chemistry. *Rev. Mod. Phys.*, 92:015003, 2020.
- [7] Yudong Cao, Jonathan Romero, Jonathan P Olson, Matthias Degroote, Peter D Johnson, Mária Kieferová, Ian D Kivlichan, Tim Menke, Borja Peropadre, Nicolas PD Sawaya, et al. Quantum chemistry in the age of quantum computing. *Chem. Rev.*, 119:10856–10915, 2019.
- [8] John Preskill. Quantum computing in the NISQ era and beyond. *Quantum*, 2:79, 2018.
- [9] Kishor Bharti, Alba Cervera-Lierta, Thi Ha Kyaw, Tobias Haug, Sumner Alperin-Lea, Abhinav Anand, Matthias Degroote, Hermanni Heimonen, Jakob S. Kottmann, Tim Menke, Wai-Keong Mok, Sukin Sim, Leong-Chuan Kwek, and Alán Aspuru-Guzik. Noisy intermediate-scale quantum (NISQ) algorithms. arXiv:2101.08448v1 [quant-ph], 2021.
- [10] Emanuel Knill, Raymond Laflamme, and Wojciech H Zurek. Resilient quantum computation. *Science*, 279:342–345, 1998.
- [11] Sergey Bravyi, Matthias Englbrecht, Robert König, and Nolan Peard. Correcting coherent errors with surface codes. *npj Quantum Inf.*, 4:1–6, 2018.
- [12] Heinz-Peter Breuer, Francesco Petruccione, et al. *The theory of open quantum systems*. Oxford University Press on Demand, 2002.

- [13] Ulrich Weiss. *Quantum dissipative systems*. World Scientific, Singapore, 2012.
- [14] Roberta Croce and Herbert van Amerongen. Light harvesting in oxygenic photosynthesis: Structural biology meets spectroscopy. *Science*, 369:933, 2020.
- [15] Eric A Arsenault, Yusuke Yoneda, Masakazu Iwai, Krishna K Niyogi, and Graham R Fleming. Vibronic mixing enables ultrafast energy flow in light-harvesting complex II. *Nat. Commun.*, 11:1460, 2020.
- [16] Lili Wang, Marco A Allodi, and Gregory S Engel. Quantum coherences reveal excited-state dynamics in biophysical systems. *Nat. Rev. Chem.*, 3:477 – 490, 2019.
- [17] Shahnawaz Rafiq and Gregory D Scholes. From fundamental theories to quantum coherences in electron transfer. *J. Am. Chem. Soc.*, 141:708 – 722, 2019.
- [18] Tae Wu Kim, Sunhong Jun, Yoonhoo Ha, Rajesh K. Yadav, Abhishek Kumar, Chung-Yul Yoo, Inhwan Oh, Hyung-Kyu Lim, Jae Won Shin, Ryong Ryoo, Hyungjun Kim, Jeongho Kim, Jin-Ook Baeg, and Hyotcherl Ihee. Ultrafast charge transfer coupled with lattice phonons in two-dimensional covalent organic frameworks. *Nat. Commun.*, 10:1873, 2019.
- [19] Wojciech Hubert Zurek. Decoherence, einselection, and the quantum origins of the classical. *Rev. Mod. Phys.*, 75:715, 2003.
- [20] Yoshitaka Tanimura and Ryogo Kubo. Time evolution of a quantum system in contact with a nearly Gaussian-Markoffian noise bath. *J. Phys. Soc. Jpn.*, 58:101, 1989.
- [21] Yoshitaka Tanimura. Stochastic Liouville, Langevin, Fokker–Planck, and master equation approaches to quantum dissipative systems. *J. Phys. Soc. Jpn.*, 75:082001, 2006.
- [22] Akihito Ishizaki and Graham R Fleming. Unified Treatment of Quantum Coherent and Incoherent Hopping Dynamics in Electronic Energy Transfer: Reduced Hierarchy Equation Approach. *J. Chem. Phys.*, 130:234111, 2009.
- [23] Jinshuang Jin, Xiao Zheng, and YiJing Yan. Exact Dynamics of Dissipative Electronic Systems and Quantum Transport: Hierarchical Equations of Motion Approach. *J. Chem. Phys.*, 128:234703, 2008.
- [24] Sabrina Maniscalco, Jyrki Piilo, F Intravaia, F Petruccione, and A Messina. Simulating quantum Brownian motion with single trapped ions. *Phys. Rev. A*, 69:052101, 2004.
- [25] Julio T Barreiro, Markus Müller, Philipp Schindler, Daniel Nigg, Thomas Monz, Michael Chwalla, Markus Hennrich, Christian F Roos, Peter Zoller, and Rainer Blatt. An open-system quantum simulator with trapped ions. *Nature*, 470:486–491, 2011.

- [26] Sarah Mostame, Patrick Rebentrost, Alexander Eisfeld, Andrew J Kerman, Dimitris I Tsomokos, and Alán Aspuru-Guzik. Quantum simulator of an open quantum system using superconducting qubits: exciton transport in photosynthetic complexes. *New J. Phys.*, 14:105013, 2012.
- [27] Anton Potočnik, Arno Bargerbos, Florian AYN Schröder, Saeed A Khan, Michele C Collodo, Simone Gasparinetti, Yves Salathé, Celestino Creatore, Christopher Eichler, Hakan E Türeci, et al. Studying light-harvesting models with superconducting circuits. *Nat. Commun.*, 9:1–7, 2018.
- [28] Bi-Xue Wang, Ming-Jie Tao, Qing Ai, Tao Xin, Neill Lambert, Dong Ruan, Yuan-Chung Cheng, Franco Nori, Fu-Guo Deng, and Gui-Lu Long. Efficient quantum simulation of photosynthetic light harvesting. *npj Quantum Inf.*, 4:1–6, 2018.
- [29] Nils Trautmann and Philipp Hauke. Trapped-ion quantum simulation of excitation transport: Disordered, noisy, and long-range connected quantum networks. *Phys. Rev. A*, 97:023606, 2018.
- [30] Christine Maier, Tiff Brydges, Petar Jurcevic, Nils Trautmann, Cornelius Hempel, Ben P Lanyon, Philipp Hauke, Rainer Blatt, and Christian F Roos. Environment-assisted quantum transport in a 10-qubit network. *Phys. Rev. Lett.*, 122:050501, 2019.
- [31] Hong-Yi Su and Ying Li. Quantum algorithm for the simulation of open-system dynamics and thermalization. *Phys. Rev. A*, 101:012328, 2020.
- [32] Guillermo García-Pérez, Matteo AC Rossi, and Sabrina Maniscalco. Ibm q experience as a versatile experimental testbed for simulating open quantum systems. *npj Quantum Inf.*, 6:1–10, 2020.
- [33] Andrea Chiuri, Chiara Greganti, Laura Mazzola, Mauro Paternostro, and Paolo Mataloni. Linear optics simulation of quantum non-markovian dynamics. *Sci. Rep.*, 2:1–5, 2012.
- [34] Richard P Feynman. Simulating physics with computers. *Int. J. Theor. Phys.*, 21:467–488, 1982.
- [35] Seth Lloyd. Universal quantum simulators. *Science*, pages 1073–1078, 1996.
- [36] PV Klimov, Julian Kelly, Z Chen, Matthew Neeley, Anthony Megrant, Brian Burkett, Rami Barends, Kunal Arya, Ben Chiaro, Yu Chen, et al. Fluctuations of energy-relaxation times in superconducting qubits. *Phys. Rev. Lett.*, 121:090502, 2018.

- [37] Jonathan J Burnett, Andreas Bengtsson, Marco Scigliuzzo, David Neepe, Marina Kudra, Per Delsing, and Jonas Bylander. Decoherence benchmarking of superconducting qubits. *njp Quantum Inf.*, 5:1–8, 2019.
- [38] Elliott Lieb, Theodore Schultz, and Daniel Mattis. Two soluble models of an antiferromagnetic chain. *Ann. Phys.*, 16:407–466, 1961.
- [39] Guang Hao Low and Isaac L Chuang. Optimal hamiltonian simulation by quantum signal processing. *Phys. Rev. Lett.*, 118:010501, 2017.
- [40] IBM quantum experience. <https://quantum-computing.ibm.com/>.
- [41] David C McKay, Christopher J Wood, Sarah Sheldon, Jerry M Chow, and Jay M Gambetta. Efficient Z gates for quantum computing. *Phys. Rev. A*, 96:022330, 2017.
- [42] J True Merrill and Kenneth R Brown. Progress in compensating pulse sequences for quantum computation. *Adv. Phys. Chem.*, pages 241–294, 2014.
- [43] Masoud Mohseni, Patrick Rebentrost, Seth Lloyd, and Alan Aspuru-Guzik. Environment-assisted quantum walks in photosynthetic energy transfer. *J. Chem. Phys.*, 129:174106, 2008.
- [44] Hung-Tzu Chang and Yuan-Chung Cheng. Coherent versus incoherent excitation energy transfer in molecular systems. *J. Chem. Phys.*, 137:165103, 2012.
- [45] Johan Strümpfer and Klaus Schulten. Open quantum dynamics calculations with the hierarchy equations of motion on parallel computers. *J. Chem. Theory Comput.*, 8:2808–2816, 2012.
- [46] Javier Cerrillo and Jianshu Cao. Non-Markovian dynamical maps: numerical processing of open quantum trajectories. *Phys. Rev. Lett.*, 112:110401, 2014.
- [47] Masoud Mohseni, AT Rezakhani, and DA Lidar. Quantum-process tomography: Resource analysis of different strategies. *Phys. Rev. A*, 77:032322, 2008.
- [48] David Gross, Yi-Kai Liu, Steven T Flammia, Stephen Becker, and Jens Eisert. Quantum state tomography via compressed sensing. *Phys. Rev. Lett.*, 105:150401, 2010.
- [49] A Shabani, RL Kosut, M Mohseni, H Rabitz, MA Broome, MP Almeida, A Fedrizzi, and AG White. Efficient measurement of quantum dynamics via compressive sensing. *Phys. Rev. Lett.*, 106:100401, 2011.
- [50] Jacob T Seeley, Martin J Richard, and Peter J Love. The Bravyi-Kitaev transformation for quantum computation of electronic structure. *J. Chem. Phys.*, 137:224109, 2012.
- [51] Héctor Abraham et al. Qiskit: An open-source framework for quantum computing. DOI: 10.5281/zenodo.2562110, 2019.

**Supplementary Information:**  
**Efficient Quantum Simulation of Open Quantum System Dynamics**  
**on Noisy Quantum Computers**

Shin Sun, Li-Chai Shih, and Yuan-Chung Cheng\*

*Department of Chemistry, National Taiwan University, Taipei City 106, Taiwan*

## CONTENTS

S1. Single qubit dynamics under $(X)^2$ gates	2
S2. State purity changes under $(X)^2$ gates	3
S3. Single qubit Bloch sphere dynamics under $(X)^2$ gates	4
S4. Noise decomposition and simulation of $(X)^2$ gates	6
S5. Compensating pulse sequence design– $(XZ)^2$ gates and $(XZXZZ)^2$ gates	8
S6. Variance of depolarizing rates of $(X)^2$ gates and $(XZXZZ)^2$ gates	12

## List of Figures

Fig. S1. Single qubit dynamics for the $(X)^2$ gates	2
Fig. S2. Single qubit purity changes for the $(X)^2$ gate	3
Fig. S3. Bloch sphere dynamics generated by applying the $(X)^2$ gate	5
Fig. S4. Fitting of the Bloch sphere dynamics for the $(X)^2$ gate	7
Fig. S5. Illustration of the compensating pulse sequences design	8
Fig. S6. Bloch sphere dynamics for the $(Z)^2$ gate	9
Fig. S7. Bloch sphere dynamics for the $(XZ)^2$ gate	10
Fig. S8. Bloch sphere dynamics for the $(XZXZZ)^2$ gate	11
Fig. S9. Depolarization rates of $(XZXZZ)^2$ and $(X)^2$ on different devices and time	12

## S1. Single qubit dynamics under $(X)^2$ gates

To investigate the qubit dynamics induced by  $(X)^2$  gates, we initialized a single qubit in the  $|0\rangle$  state and applied multiple  $(X)^2$  gates on it. Projective measurement in the computational basis is then performed to obtain the population in  $|0\rangle$  ( $P_0$ ) as a function of the number of  $(X)^2$  gates applied. Figure S1 shows population in  $|0\rangle$  as a function of the number of  $(X)^2$  gates applied. We performed the same experiment on different days as well as different qubits on the IBM-Q quantum computer. Note that  $(X)^2$  gate corresponds to the identity operation. However, in all cases, the  $P_0$  quickly decreases, and the dynamics behave as highly-noisy fluctuations tending towards the maximally disordered state ( $P_0 = 0.5$ ). We speculated that the dynamics can be explained by two predominant types of errors in the X gates. An over-rotation of the X gates results in the population change at the initial stages, and decoherent-type error dominates at large number of X gates, which in turn drives the population towards 0.5. We thus perform further state characterization to assess the dynamics of the noises induced by  $(X)^2$  gates (Secs. S2-S4). Furthermore, the population dynamics under different parameters behaves very differently even qualitatively, which also signify the highly unstable nature of the  $(X)^2$  gate noises.

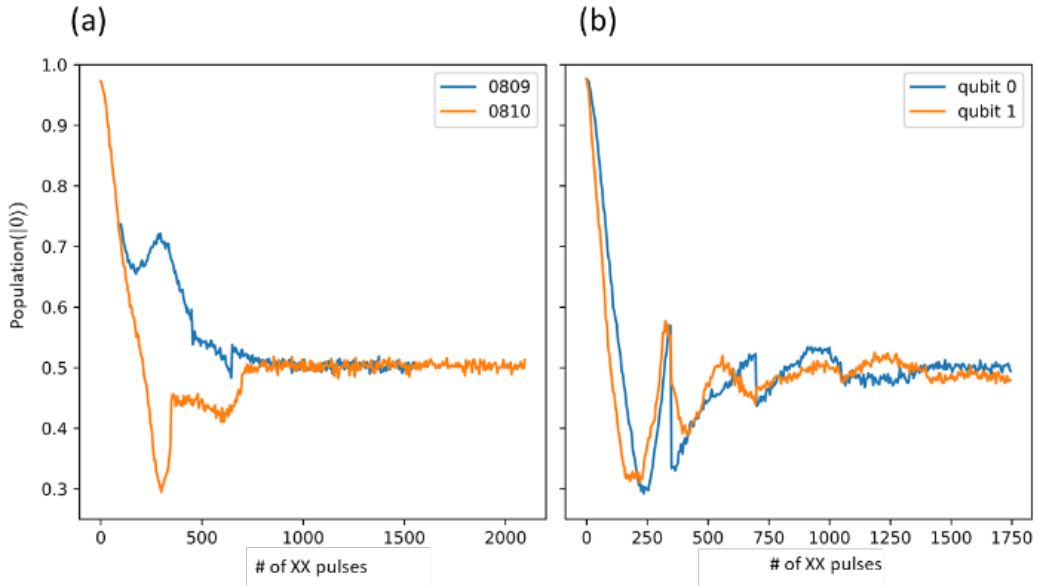


**FIG. S1. Single qubit dynamics for the  $(X)^2$  gates.** Populations of  $|0\rangle$  as functions of the number of applied  $(X)^2$  gates are plotted. (a) Results on different days (8/9 and 8/10) but on the same physical qubit. (b) Results on different physical qubits. All experiments were performed on `ibmq_ourense`

## S2. State purity changes under $(X)^2$ gates

To obtain quantitative information about the qubit coherence under  $(X)^2$  gates, we initialize the qubit in four states  $(|0\rangle, |1\rangle, |+\rangle = (|0\rangle + |1\rangle)/\sqrt{2}, |-\rangle = (|0\rangle + i|1\rangle)/\sqrt{2})$ , apply a number of  $(X)^2$  gates and measure the expectation values in the Pauli basis. Quantum state tomography is then performed to reconstruct the density matrices (2.1) at each number of  $(X)^2$  gates applied. We compute the purity  $\gamma \equiv \text{tr}(\rho^2)$  of the states to assess the coherence of qubit under  $(X)^2$  gates. Figure S2 shows the purities as functions of the number of  $(X)^2$  gates for each input state. The purities generally decrease as the increasing number of  $(X)^2$  gates, but the decaying rates are different for each initial state, suggesting that the decoherence errors are state-dependent. The purity information thus provides a direct evidence of the decoherence error introduced by the  $(X)^2$  gates.

$$\rho = \frac{I + \text{tr}(\rho \sigma_x) \sigma_x + \text{tr}(\rho \sigma_y) \sigma_y + \text{tr}(\rho \sigma_z) \sigma_z}{2} \quad (2.1)$$

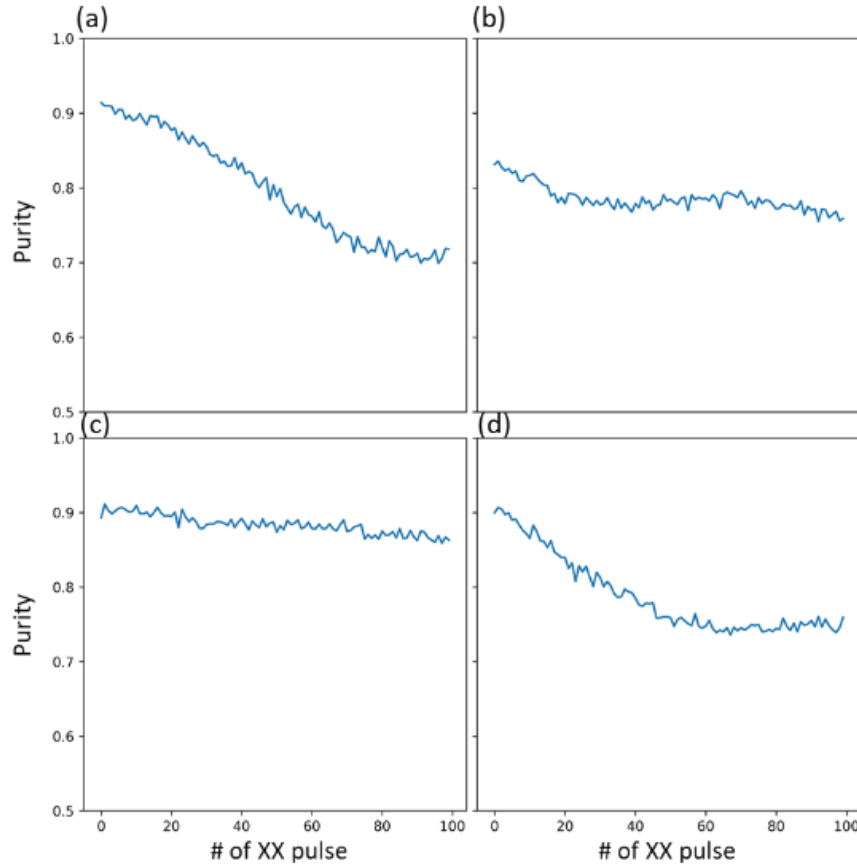


**FIG. S2. Single qubit purity changes for the  $(X)^2$  gate.** The state purity as functions of the number of applied  $(X)^2$  gates is plotted. (a) – (d) corresponds to initial state  $= |0\rangle, |1\rangle, |+\rangle, |-\rangle$ , respectively. All experiments were performed on `ibmq_bogota`.

### S3. Single qubit Bloch sphere dynamics under $(X)^2$ gates

Here we visualize the noise induced by  $(X)^2$  gates by plotting the single qubit dynamics as a function of the number of  $(X)^2$  applied. We performed quantum state tomography to obtain the quantum states for four different input state ( $|0\rangle$ ,  $|1\rangle$ ,  $|+\rangle$ ,  $|-\rangle$ ). By decomposing the single qubit density matrix with respect to Pauli basis (3.1), we can obtain the Bloch vector representation  $(r_x, r_y, r_z)$  of the qubit state.

$$\rho = \frac{I + r_x \sigma_x + r_y \sigma_y + r_z \sigma_z}{2} \quad (3.1)$$

Because we perform the input-output analysis in a tomographically-complete bases, the procedure is also equivalent to quantum process tomography, and it provides an intuitive understanding about the underlying qubit dynamics when presented on a Bloch sphere. Figure S3 shows the  $(X)^2$  dynamics for different initial states. The Bloch vector for the single qubit state is represented by a dot, and the dot is traced continuously with increasing number of  $(X)^2$  gates. For each input state, the dynamics could be seen as rotations around the X axis (arising from the over-rotation of X gates), plus an uniform contraction towards the center (typical behavior for the depolarizing noises). It is worth noting that for the initial state  $|+\rangle$ , being the eigenstate of the X-rotation, shows only contraction.

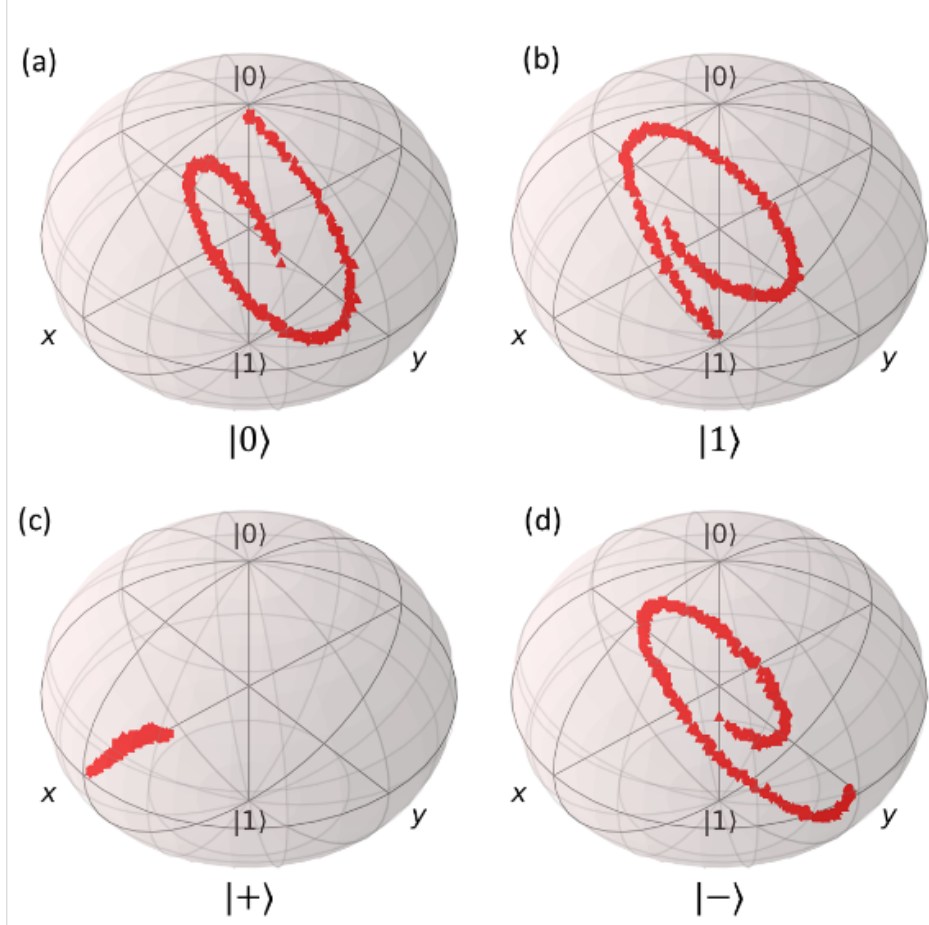


**FIG. S3. Bloch sphere dynamics generated by applying the  $(X)^2$  gate.** We initialize the qubit in different initial states,  $|0\rangle, |1\rangle, |+\rangle, |-\rangle$ , and apply  $(X)^2$  gates from 0~300 times to analyze the dynamics. The Bloch vector for the single qubit state is represented by a dot, and the dot is traced continuously with increasing number of  $(X)^2$  gates. (a)-(d) all show the effect of rotating around the X axis and shortening towards the center. All experiments were performed on `ibmq_manhattan`.

## S4. Noise decomposition and simulation of $(X)^2$ gates

To quantitatively analyze the qubit dynamics generated by the  $(X)^2$  gate, we build simple mathematical models to describe them. As in Sec. 3 suggests, the quantum process could be seen as a combination of systematic coherent rotation together with depolarization error. In the following experiments, we thus use operator sum representation (4.1) to numerically propagate the qubit states and fit the dynamics obtained (with initial state  $=|0\rangle$ ) in Sec.3 on IBMQ.

$$E(\rho) = \sum_k E_k \rho E_k^\dagger \quad (4.1)$$

where  $E_k$  are operation elements, satisfying  $\sum_k E_k E_k^\dagger = I$ .

We took both coherent rotation (4.2) and depolarization (4.3) into account in our model (The free parameters are rotation angle step  $\theta$  and depolarizing probability  $p$ ).

$$E_0 = e^{-\frac{i\theta X}{2}} = \cos \frac{\theta}{2} I - i \sin \frac{\theta}{2} X = \begin{bmatrix} \cos \frac{\theta}{2} & -i \sin \frac{\theta}{2} X \\ -i \sin \frac{\theta}{2} X & \cos \frac{\theta}{2} \end{bmatrix} \quad (4.2)$$

$$E_1 = \sqrt{1 - \frac{3p}{4}} \begin{bmatrix} 1 & 0 \\ 0 & 1 \end{bmatrix}, \quad E_2 = \sqrt{\frac{p}{4}} \begin{bmatrix} 1 & 0 \\ 0 & 1 \end{bmatrix}, \quad E_3 = \sqrt{\frac{p}{4}} \begin{bmatrix} 1 & -i \\ i & 1 \end{bmatrix}, \quad E_4 = \sqrt{\frac{p}{4}} \begin{bmatrix} 1 & 0 \\ 0 & -1 \end{bmatrix} \quad (4.3)$$

In Fig. S4, we plot both the Bloch sphere dynamics for the  $(X)^2$  gates (red dots), and the fitted dynamics (green). It can be noted that the parameters suitable for the (a) case, cannot reproduce the dynamics for other states (b-d) well for long time. This suggests the state-dependent nature of the quantum gate noises, and could be investigated in the future.

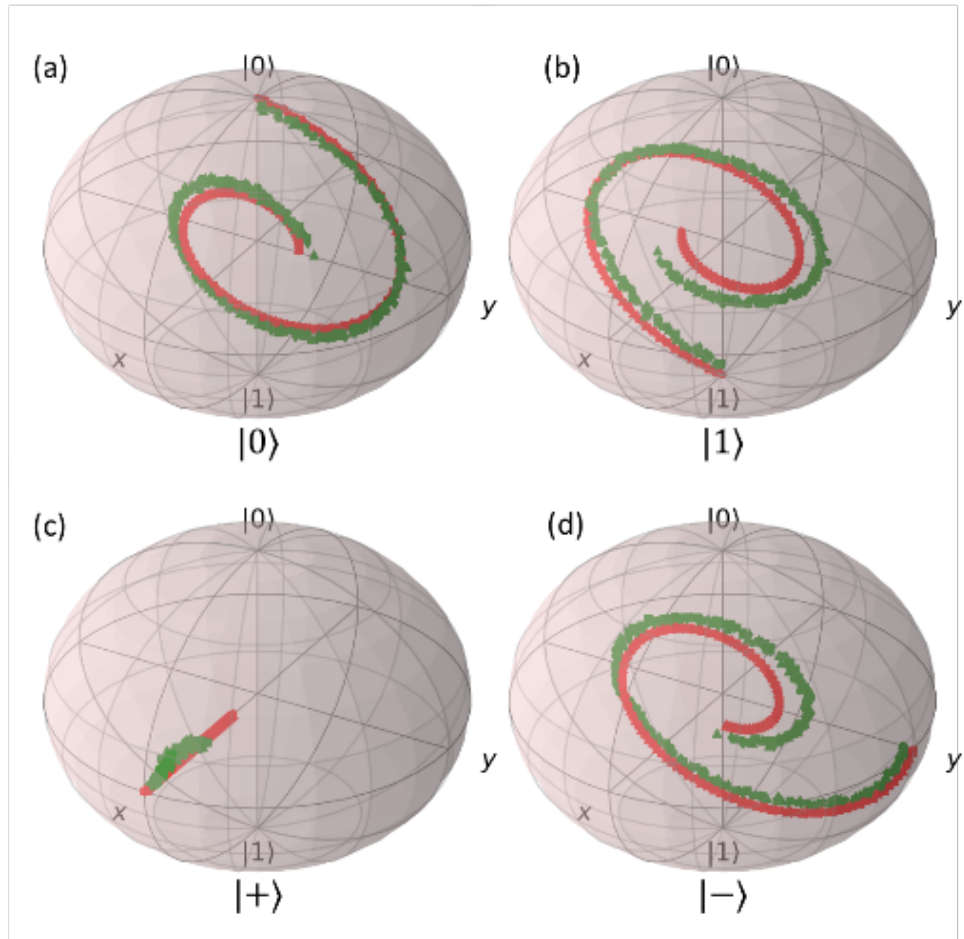


**FIG. S4. Fitting of the Bloch sphere dynamics for the  $(X)^2$  gate.**

The Bloch sphere dynamics for the  $(X)^2$  gate (red) in Fig. S3 are fitted with qubit dynamics with rotation angle step  $\theta = 0.013$  and depolarization probability  $p = 0.005$ .

### S5. Compensating pulse sequence design – $(XZ)^2$ , $(XZXZZ)^2$ gates

In order to adaptively eliminate the over-rotation in the  $(X)^2$  gate without knowing the over-rotation angle in advance, we resort to the echo-type techniques to correct the coherent error (Fig. S5). We first assess the Bloch sphere dynamics of multiple Z gates (Fig. S6) to make sure they do not introduce excess error by themselves.

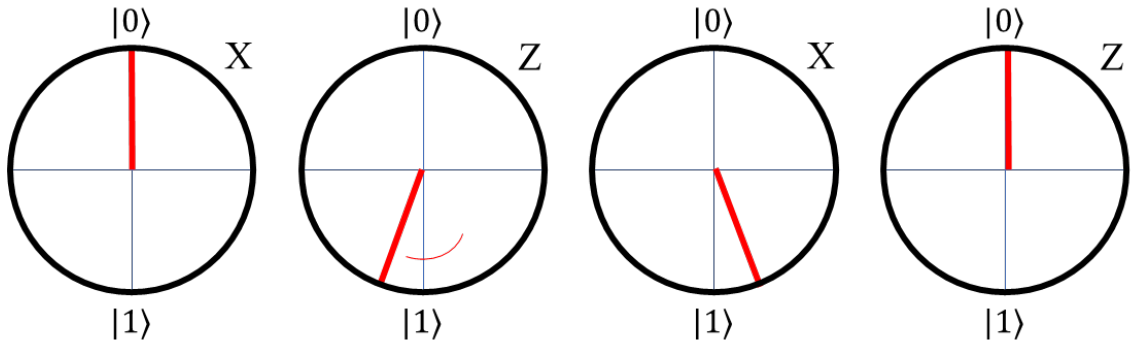


FIG. S5. **Illustration of the compensating pulse sequences design.** The circle is a projection of the Bloch sphere on YZ-plane. To dynamically correct the over-rotation error, first, a X gate is applied. The over-rotation is then turned into an under-rotation by applying a phase (Z) gate. The over-rotation of the second applying X gates then cancels the under-rotation. Finally, another Z gate is applied to recover identity.

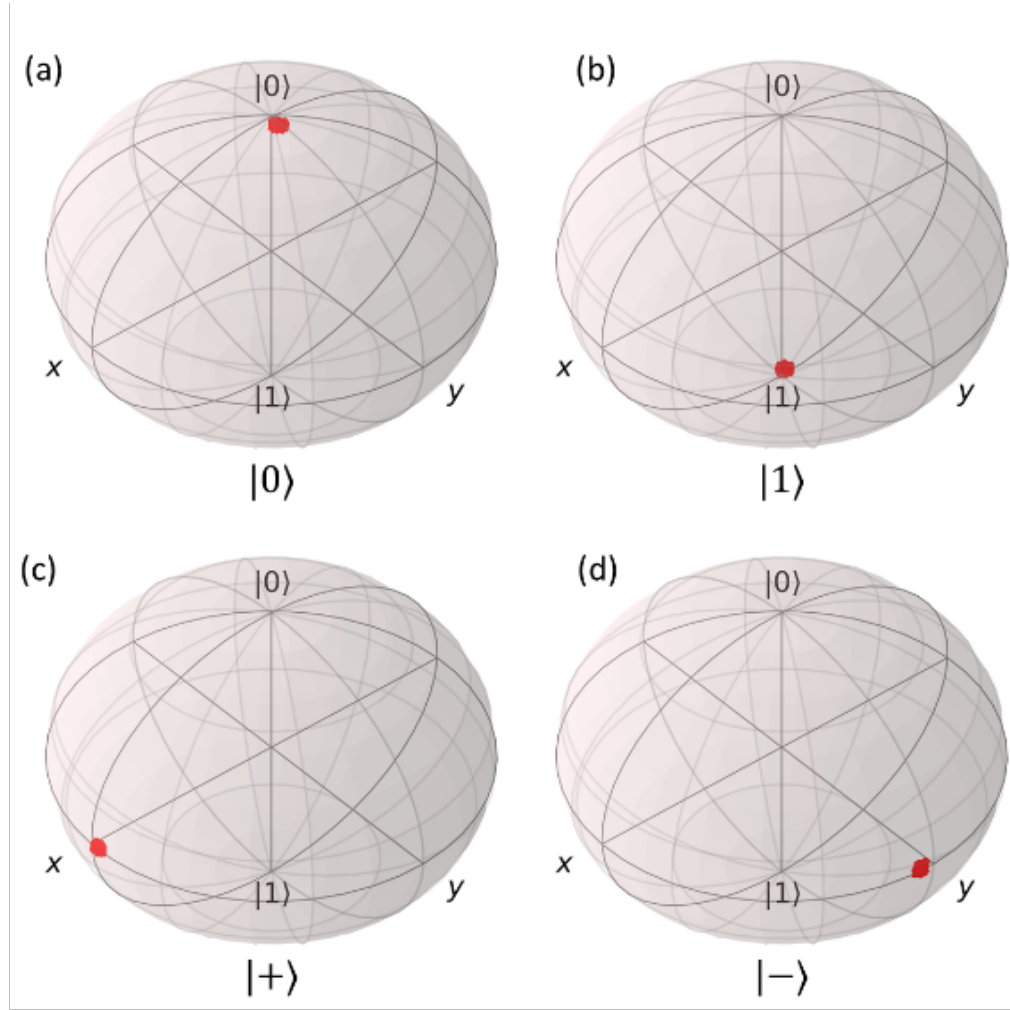
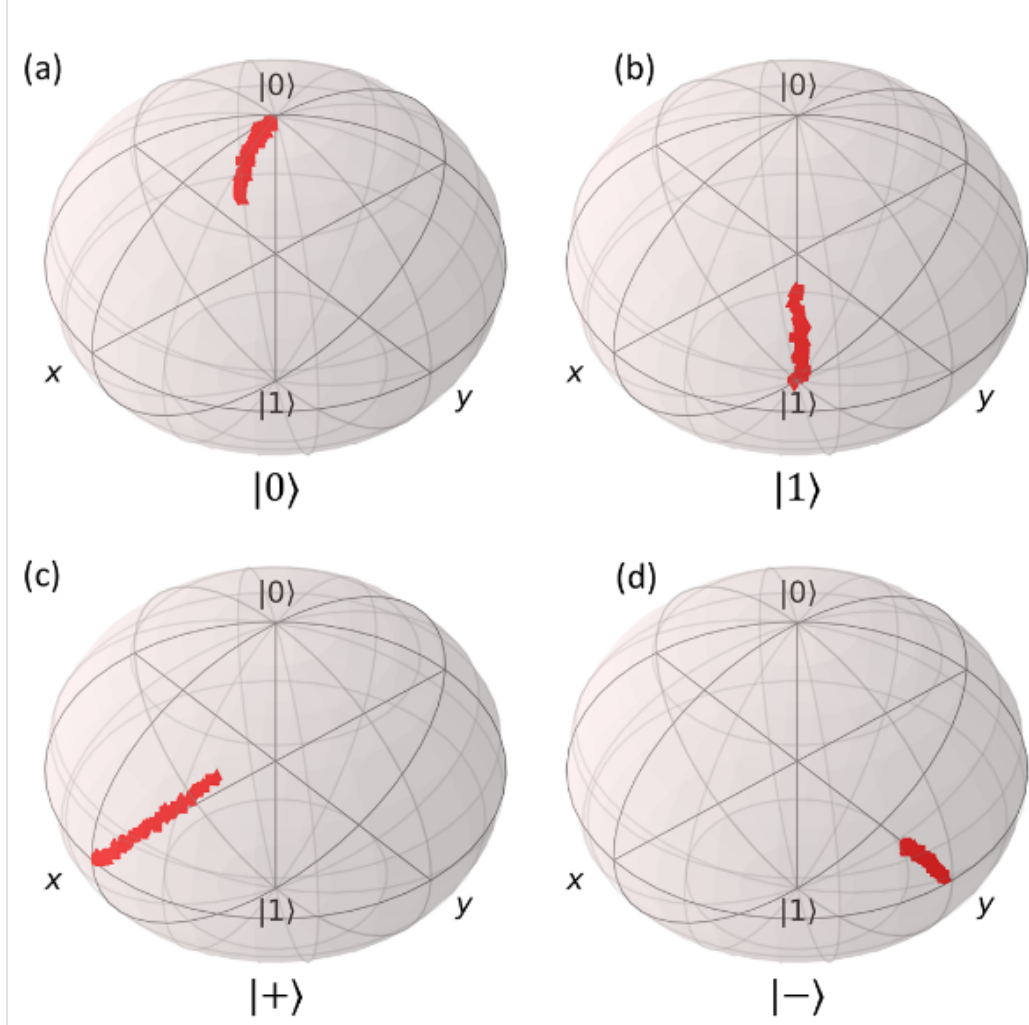


FIG. S6. **Bloch sphere dynamics for the  $(Z)^2$  gate.** We initialize the qubit in four basis state, and apply  $(Z)^2$  gates from 0~100 times to analyze their behaviors. Each point on the Bloch Sphere represent the density matrix at each number of applied  $(Z)^2$  gates. Experiments were performed on [ibmq\\_paris](#).

We then assess the dynamics of  $(XZ)^2$  gates by following the same procedure as in Sec. S3. The results are again plotted in Fig. S7. For the input states  $|0\rangle$  (Fig. S7 (a)), the dynamics still contain a systematic rotation part. We proposed that this is due to the phase error in the Z gates, which still causes systematic rotations. Therefore, we chose to compensate the systematic rotation again by adopting the  $(XZXZZ)^2$  gates.



**FIG. S7. Bloch sphere dynamics for the  $(XZ)^2$  gate.** We initialize the qubit in four basis state, and apply  $(XZ)^2$  gates from 0~100 times to analyze their behaviors. Each point on the Bloch Sphere represent the density matrix at each number of applied  $(XZ)^2$  gates. In the case of (a) , a systematic rotation is still present. Experiments were performed on `ibmq_paris`.

Furthermore, in the case of  $(XZXZZ)^2$ , it can be seen from the Bloch sphere dynamics (Fig. S8) that for all input states, the systematic rotation in the dynamics is much eliminated. Thus, the  $(XZXZZ)^2$  can be regarded as good decoherence-inducing gate for our purpose to introduce dissipation into the model system in the main text.

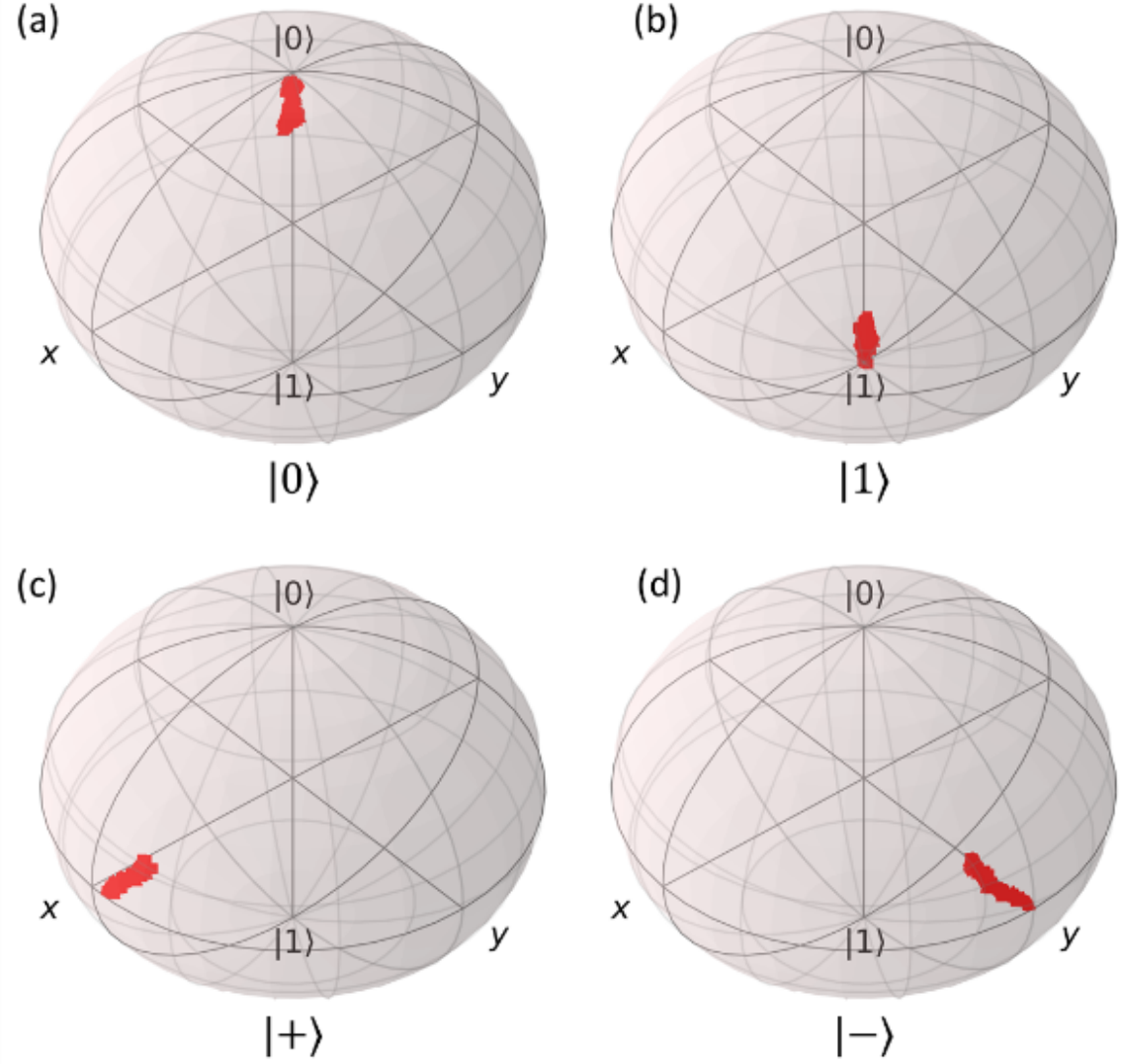


**FIG. S8. Bloch sphere dynamics for the  $(XZXZZ)^2$  gate.** We initialize the qubit in four basis state, and apply  $(XZXZZ)^2$  gates from 0~100 times to analyze their behaviors. Each point on the Bloch Sphere represent the density matrix at each number of applied  $(XZ)^2$  gates. Experiments were performed on `ibmq_manhattan`.

## S6. Variance of depolarizing rates of $(XZXZZ)^2$ and $(X)^2$

Here we assess the fluctuation of the decoherence noise strengths for the single-qubit decoherence-inducing gates. To this end, we perform state tomography to obtain single qubit Bloch sphere dynamics under  $(XZXZZ)^2$  and  $(X)^2$  gate sequences, and fit the dynamics with our model as in Sec.4. We then extract the depolarization rate and assess their behaviors on different devices and days (Fig. S9). Three consecutive experiments were performed and fitted independently to support a statistical analysis. For the  $(XZXZZ)^2$  case, the depolarization rate shows a consistent trend among devices (Fastest: Manhattan, Slowest: Bogota). In the case of manhattan, the depolarization rate exhibited large fluctuations, and are not significantly different across days. In the case of paris and bogota, the deviation of noises was much smaller, suggesting the stability of the noises under  $(XZXZZ)^2$  were better than manhattan. Except on 12/27, the depolarization rates on three devices were all quantitatively different than others. As for the case of  $(X)^2$  gates, the depolarization rates were all smaller than that of  $(XZXZZ)^2$  due to a smaller number of pulses per identity, and the stabilities were also better in general.

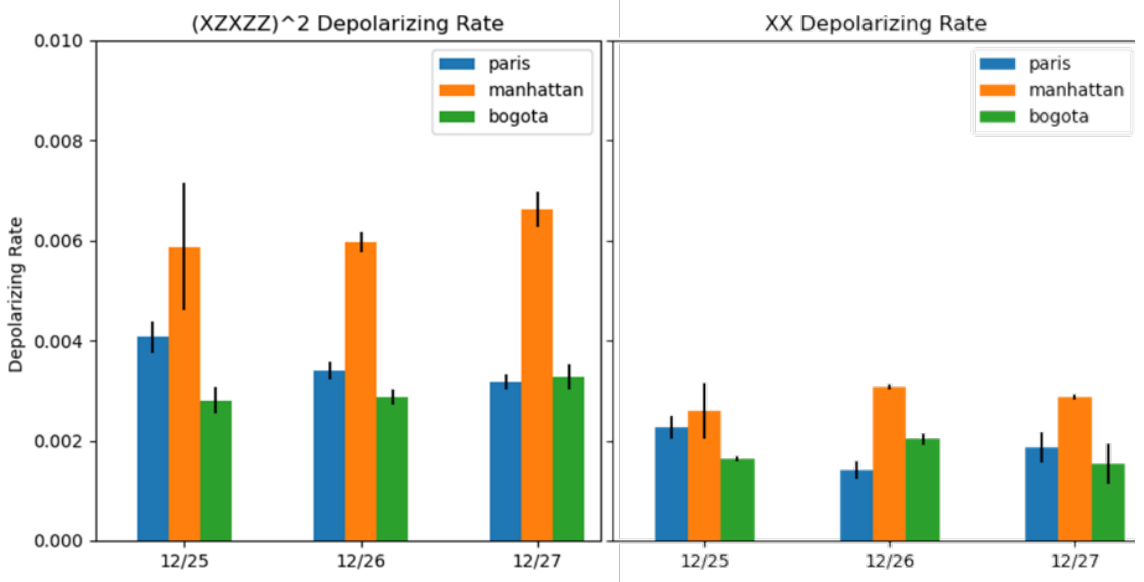


FIG. S9. **Depolarization rates of  $(XZXZZ)^2$  and  $(X)^2$  on different devices and time.** The fitted depolarization rates for the  $(XZXZZ)^2$  and  $(X)^2$  gates on different devices and days are shown. The error bars are calculated from three consecutive experiments.